Advanced Modulation Techniques for High-Performance Computing Optical Interconnects

Fotini Karinou, Robert Borkowski, Darko Zibar, Ioannis Roudas, *Member, IEEE*, Kyriakos G. Vlachos, and Idelfonso Tafur Monroy

***Abstract*—We experimentally assess the performance of a 64 × 64 optical switch fabric used for ns-speed optical cell switching in supercomputer optical interconnects. More specifically, we study four alternative modulation formats and detection schemes, namely, 10-Gb/s nonreturn-to-zero differential phase-shift keying with balanced direct detection, 10-Gb/s polarization division multiplexed (PDM) quadrature phase-shift keying, 40-Gb/s single-polarization 16-ary quadrature amplitude modulation (16QAM), and 80-Gb/s PDM-16QAM, with coherent intradyne detection, in conjunction with an optimized version of the optical shared memory supercomputer interconnect system switch fabric. In particular, we investigate the resilience of the aforementioned advanced modulation formats to the nonlinearities of semiconductor optical amplifiers, used as ON/OFF gates in the supercomputer optical switch fabric under study. In addition, we compare their performance using as a benchmark the performance of conventional 10-Gb/s intensity modulation direct detection (IM/DD). We show that the choice of the appropriate advanced modulation format can increase the capacity of the switch fabric, while, at the same time, it can mitigate the main nonlinear effect, i.e., cross-gain modulation that arises when using conventional IM/DD. Nonlinear phase distortion becomes the main limiting factor when advanced modulation formats are used.**

***Index Terms*—Optical interconnects, semiconductor optical amplifiers (SOAs), switching.**

I. Introduction

OPTICS are currently used in rack-to-rack interconnects for high-performance computing (HPC) systems [1]. State-of-the-art rack-to-rack supercomputer interconnects use electronic very large scale integration CMOS switch fabrics for packet switching and active optical cables for transmission [2]. The latter are based on vertical-cavity surface-emitting laser diodes (VCSELs), multimode fibers [2], and intensity modulation/direct detection (IM/DD) [1]. Advanced modulation formats have been proposed for increasing the capacity of point-to-point links in the next-generation optical interconnects [3]–[7]. Nevertheless, their deployment in future data center optical interconnects will mainly depend on the dramatic reduction of system complexity. In the more distant future, just-in-time optical packet switching might be performed using semiconductor optical amplifiers (SOAs) as ON/OFF gates [8]–[10]. For instance, several optical interconnects based on SOAs have already been demonstrated in [8], [11]–[13]. Representative examples are the Data Vortex [14]–[15] and the optical shared memory supercomputer interconnect system (OSMOSIS) [16] switch fabric architectures.

The OSMOSIS project [16] originally proposed a bufferless crossbar optical switch fabric implemented using a broadcast-and-select network architecture with fixed wavelength transmitters and discretely tunable receivers. In the previous architecture, each receiver card used a SOA-based, two-stage wavelength selector to perform switching. In a subsequent study, we proposed the substitution of the original two-stage wavelength selectors by multistage wavelength selectors exploiting the cyclic properties of arrayed waveguide (AWG) multiplexers/demultimplexers (MUX/DMUXs) to reduce the number of ON/OFF gates to a minimum [17]–[18]. In the latter architecture, SOA concatenation results in the accumulation of amplified spontaneous emission (ASE) noise and, most importantly, in distortion due to nonlinear effects, especially self-gain (SGM) and cross-gain modulation (XGM) [19]–[20]. These effects limit the maximum number of channel selection stages on the receiver cards and, eventually, the size of the optical interconnect.

The use of advanced modulation formats, such as return-to-zero (RZ) differential phase-shift keying (DPSK) [21]–[24], RZ differential quadrature phase-shift keying (RZ-DQPSK) [20], polarization shift keying [25], polarization-bit-interleaved RZ-DQPSK [20], or polarization division multiplexed (PDM) quadrature phase-shift keying (PDM-QPSK) [26]–[27], has been proposed to mitigate nonlinear effects, such as XGM, in SOAs. Nevertheless, different nonlinear effects induced by SOAs, i.e., cross-phase modulation (XPM), are pronounced in that case [28]–[31].

In [10], we compared the performance of two versions of the 64 × 64 OSMOSIS wavelength-space switch fabric, the one originally proposed in [16] and its optimized version (in terms of active component count) proposed in [17] and [18], assuming 10-Gb/s IM/DD links. In a different study [26], we explored the use of coherent PDM-QPSK to reduce the impact of the transmission effects in the aforementioned optical switch fabric. Unfortunately, in this early study, experimental results suffered from severe phase noise limitations due to the broad

Manuscript received June 1, 2012; revised August 13, 2012, September 13, 2012, and November 5, 2012; accepted November 26, 2012. Date of publication December 3, 2012; date of current version April 3, 2013.

F. Karinou, I. Roudas, and K. G. Vlachos are with the University of Patras, Patras 26500, Greece (e-mail: karinou@ece.upatras.gr; roudas@ece.upatras.gr; kvlachos@ceid.upatras.gr).

R. Borkowski, D. Zibar, and I. Tafur Monroy are with the DTU Fotonik, Department of Photonics Engineering, Technical University of Denmark, 2800 Kongens Lyngby, Denmark (e-mail: rbor@fotonik.dtu.dk; idtm@fotonik.dtu.dk; dazi@fotonik.dtu.dk).

Color versions of one or more of the figures in this paper are available online at http://ieeexplore.ieee.org.

Digital Object Identifier 10.1109/JSTQE.2012.2231405

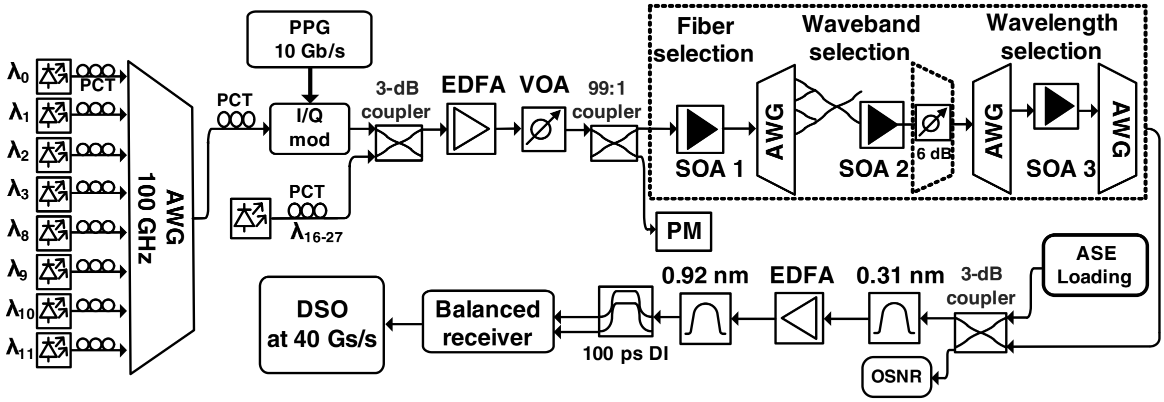

Fig. 1. Experimental setup for the investigation of the performance of 10-Gb/s NRZ-DPSK in the optimized OSMOSIS 64 × 64 optical interconnect architecture. (Symbols: PCT = polarization controller, AWG = arrayed waveguide grating, I/Q mod = quadrature modulator, EDFA = erbium-doped fiber amplifier, VOA = variable optical attenuator, SOA = semiconductor optical amplifier, ASE = amplified spontaneous emission, OSNR = optical signal-to-noise ratio, DI = delay interferometer, DSO = digital sampling oscilloscope).

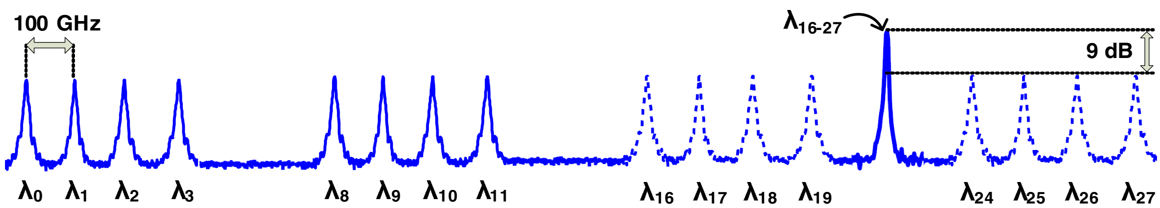

Fig. 2. Nominal (λ_0–λ_{27}) and implemented (blue solid line) wavelength allocation scheme.

3-dB linewidth (∼20 MHz) of the transmitter laser diode available in our lab.

In this paper, we study for the first time, the transmission performance of multilevel, spectrally efficient modulation formats in cell-switching interconnect architectures that employ combinations of AWGs and SOAs with different wavelength load per SOA. Moreover, critical issues such as cost, energy efficiency, forward-error correction (FEC), and latency are discussed.

More specifically, we investigate the use of advanced modulation formats, in the 64 × 64 optimized, three-stage version of the OSMOSIS optical switch fabric proposed in [17]–[18], in order to both increase the capacity of the switch [32] and counteract the nonlinearities that limit its size. In particular, first, we consider a realistic short-term solution for the choice of the modulation format, i.e., 10-Gb/s nonreturn-to-zero (NRZ) DPSK with balanced direct detection. Next, we reevaluate the performance of the interconnect when coherent PDM-QPSK is employed. The potential merit of NRZ-DPSK and PDM-QPSK lies not only in their well-known superior sensitivity and spectral efficiency, but mainly in their resilience to SOA nonlinear transmission effects (i.e., XGM) due to their envelope constancy [19]. Moreover, we test, by simulation, an alternative configuration for PDM-QPSK that uses the proposed OSMOSIS switch fabric to select the wavelength of the local oscillator (LO) for each receiver. This configuration eliminates the performance degradation due to phase noise, since it relies on self-homodyne detection. Finally, in order to further increase the capacity of the optimized OSMOSIS interconnect architecture, we investigate a futuristic scenario of employing 40-Gb/s single polarization (SP), and 80-Gb/s PDM, 16-ary quadrature amplitude modulation (16QAM) with coherent detection. Results show that the performance of transmitted channels, for all advanced modulation formats under investigation, differs by about 1 dB in terms of required optical signal-to-noise ratio (OSNR) at bit error rate (BER) equal to BER = 10^{-3}. Moreover, it is shown that NRZ-DPSK is the most resilient modulation format to SOA phase-induced nonlinearities, in the optimized OSMOSIS 64 × 64 switch fabric.

The remainder of this paper is organized as follows: In Section II, the experimental setups used for the evaluation of the performance of NRZ-DPSK, PDM-QPSK, and SP- and PDM-16QAM are described in detail. In Section III, performance results for the aforementioned modulation formats are presented. In Section IV, system complexity, energy efficiency, and further performance aspects are discussed.

II. Experimental Setups

A. DPSK Experimental Setup

Fig. 1 shows the experimental setup used for the investigation of the performance of 10-Gb/s NRZ-DPSK. The optimized 64 × 64 OSMOSIS switch fabric uses 64 transmitters, partitioned into four identical 16-wavelength sets [17]–[18]. Each wavelength set is partitioned into four wavebands of four wavelengths each. The full wavelength division multiplexing (WDM) signal occupies an aggregate frequency bandwidth of 2.7 THz. The wavelength allocation is shown in Fig. 2, where we chose λ_0 = 1546.897 nm in this particular case, based on the availability of components in our lab. Guard bands facilitate waveband multiplexing/demultiplexing. The channel spacing within a waveband is Δf = 100 GHz. The channel spacing of the WDM signal was kept at 100 GHz during all experiments to match the ITU grid and the available laboratory equipment. The guard band between two adjacent wavebands was also chosen to match the free spectral range of the experimentally available AWG MUXs/DMUXs. The impact of interchannel nonlinear phenomena, such as XGM, XPM, and four-wave mixing (FWM), becomes less important as the channel spacing increases [22], [33]. Therefore, we would expect better performance for larger, e.g., 200-GHz channel spacing. Nevertheless, in that case, the spectral occupancy would be of the order of 5.4 THz (given the wavelength allocation shown in Fig. 2, the channel spacing, and the same bandwidth/guard-band ratios for the AWGs), instead of 2.7 THz for the 100-GHz channel spacing currently used. To avoid such poor spectral occupancy, 100 GHz seems to be a reasonable choice. On the other hand, a denser frequency grid, e.g., 50 GHz, would result in a stronger impact of interchannel nonlinear phenomena and in adjacent-channel crosstalk [20] (albeit small for 10 Gb/s signals but significant for the 40 Gb/s signals used in the original OSMOSIS test bed [16]). In this case, performance would deteriorate due to FWM, compared to the performance for the 100-GHz channel spacing case, where no FWM products have been observed experimentally. In conclusion, 100-GHz channel spacing was chosen because it is considered a reasonable and satisfactory tradeoff between interchannel nonlinearities and spectral occupancy.

In the experimental setup, due to lack of components, only nine lasers (shown with solid lines in Fig. 2), are used. The first eight wavelengths fully populate the first two wavebands used in the optimized 64 × 64 OSMOSIS switch fabric architecture [17], [18]. These are multiplexed using an AWG MUX and, subsequently, they are modulated using a 10-Gb/s 2^{15}–1 pseudorandom binary sequence (PRBS), to form eight identical NRZ-DPSK signals. Semiconductor lasers in the two remaining wavebands W_3–W_4, i.e., λ_{16}–λ_{27} (shown with dashed lines in Fig. 2) are not available in our lab. They are emulated by a single continuous wave (CW) laser source with eight times the nominal power of a single channel, placed in the middle of W_3–W_4 (see Fig. 2). We should note here that the CW signal will act to increase the carrier recovery rate, so it replicates the case that eight independent wavelengths are used. In these terms, it emulates the actual relation between gain saturation and total input power. It is a good approximation to account for the saturation in the SOA in case of eight further channels. Moreover, the crosstalk induced by the wavelengths belonging to W_3 and W_4 do not have a significant contribution in crosstalk in wavelengths of W_1 and W_2 as they are placed 400 GHz (for λ_{16}) to 1.2 THz (for λ_{27}) far away in case of the closest neighboring implemented wavelength λ_{11} under investigation. Crosstalk for the channels under investigation is taken into account by the eight spectrally close and modulated signals. In these terms, we believe it is a fair approximation, given that it is similarly repeated for all three experimental setups (see Sections II-A–II-C).

All nine wavelengths are combined together using a coupler. Then, the WDM signal is amplified by an erbium-doped fiber amplifier (EDFA) and attenuated by a variable optical attenuator (VOA), representing the 1:64 star coupler of the actual OSMOSIS switch fabric architecture [16]. A 99:1 coupler is used to monitor the input power into the first SOA, which is optimized so that the SOAs work approximately in the linear regime, close to saturation. We should note here that there is no decorrelation of the modulated signals at the input of the first SOA. Next, the signals pass through three consecutive wavelength selection stages employing SOAs as ON–OFF gates. The SOAs in the experiment are 1 mm long, with a 3-dB bandwidth of 90 nm, a small-signal gain of 15 dB, a high input saturation power of approximately 4 dBm, and a low polarization-dependent gain (PDG) of less than 0.2 dB [10]. The first SOA is used to select one out of four fibers. The waveband selection stage should ideally consist of a pair of 400-GHz MUX/DMUX interconnected with four SOAs, acting as ON/OFF gates [17]–[18]. In our experiment, due to lack of resources, it consists of a 100-GHz AWG MUX with interconnected arms to emulate the 400-GHz MUX required in the proposed architecture [17]–[18], a single SOA, and a 6-dB attenuator to emulate another 400-GHz AWG MUX, not available in the lab. The selection of the desired wavelength is performed by a third selection stage, which is comprised of a pair of conventional AWG MUX/DMUX, with 100 GHz spacing, and a single SOA. The net gain of the three stages is 11, 5, and 5 dB, for the first, second, and third stage, respectively. In the OSMOSIS interconnect, temperature stabilization of all lasers, SOAs, and AWG MUX/DMUXs is assumed. The impact of laser/filter frequency misalignments was not taken into account in this study. We assumed that any potential drift of the laser carrier frequency by environmental temperature, etc., would not be strong enough to shift a significant portion of the signal spectrum out of the bandpass of AWG MUX/DMUXs, as the AWG 3-dB channel bandwidth is $\sim$77 GHz ($\sim$0.6 nm). Judging by typical characteristics of a commercial off-the-shelf distributed-feedback (DFB) laser, the 77-GHz AWG channel corresponds to a drift of $\sim$5 °C, which is highly unlikely to happen with a common temperature control for a DFB laser bank or an appropriate environmental conditioning for the data center. Furthermore, future progress in semiconductor technology might ensure stable, uncooled SOA operation as demonstrated for SOAs [34]. In addition, the electronic equalizer in the coherent receiver (see Sections II-B–II-C) is able to compensate for some excess filtering due to frequency drifts.

ASE noise is loaded after the last selection stage, in order to adjust the received OSNR. Then, the selected wavelength is filtered by a 0.31-nm bandwidth optical filter, amplified by an EDFA, and filtered again by a 0.92-nm bandwidth optical filter to reject out-of-band noise stemming from the optical preamplifier. For direct detection of DPSK signals, a 100-ps delay interferometer (DI) is employed in front of a balanced receiver. The photocurrent is sampled using a digital sampling oscilloscope (DSO) at 40 GSamples/s. BER measurements are carried out to assess the performance of the switch. BER is also measured as a function of the input power to the first SOA, in order to quantify the tolerance of the NRZ-DPSK to SOA-induced nonlinearities [20].

B. PDM-QPSK Experimental Setup

The experimental setup used for the evaluation of the performance of 10-Gb/s PDM-QPSK is shown in Fig. 3. The channel allocation scheme is the same as before (see Fig. 2). In the experiment, only eight DFB semiconductor lasers corresponding to the first two wavebands, for the wavelength range from $\lambda_0 = 1548.808$ to $\lambda_{11} = 1557.608$ nm, are used. Another DFB laser, having eight times the nominal power of each channel, is tuned at $\lambda_{17.5} = 1562.808$ nm, approximately, to represent the remaining eight channels employed in the optimized OSMOSIS optical interconnect architecture [17]–[18]. The laser source for the wavelength under test is substituted by a tunable

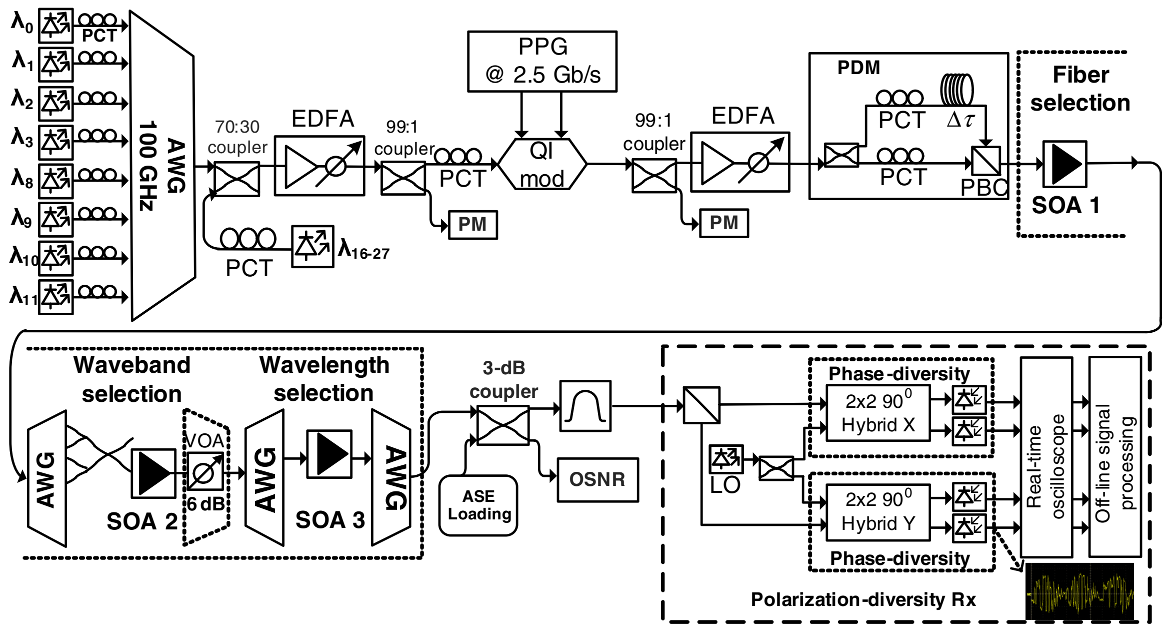

Fig. 3. Experimental setup for the investigation of the performance of 10-Gb/s PDM-QPSK in the optimized OSMOSIS 64 × 64 optical interconnect architecture. (Symbols: PCT = polarization controller, AWG = arrayed waveguide gratings, EDFA = erbium-doped fiber amplifier, PM = powermeter PPG = pattern pulse generator, QI mod = quadrature modulator, PDM = polarization division multiplexing, PBC = polarization beam combiner, SOA = semiconductor optical amplifier, ASE = amplified spontaneous emission, OSNR = optical signal-to-noise ratio, Rx = receiver).

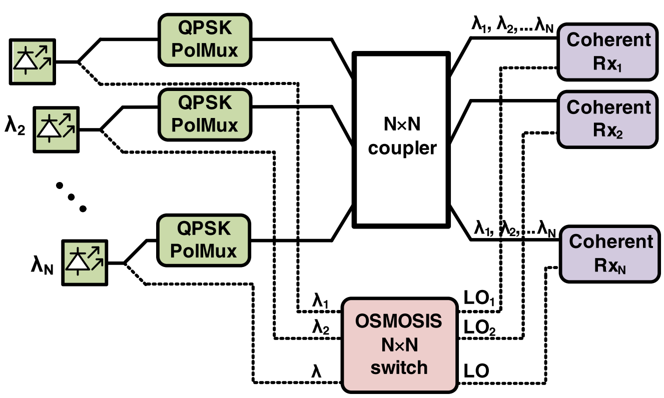

Fig. 4. Alternative $N \times N$ optical interconnect architecture, using the OSMOSIS switch fabric for the selection of the appropriate wavelength for the LO, for each one of the coherent receivers. (Symbols: LO = local oscillator, Rx = receiver).

external-cavity laser (ECL) with a 3 dB linewidth of 200 kHz. The eight channels are first multiplexed using an AWG, then are combined with $\lambda_{17.5}$ to form the WDM signal, and, finally, are amplified by a flat-gain EDFA. A VOA is used to adjust the power at the output of the EDFA. All channels are QPSK modulated using a single $LiNbO_3$ quadrature modulator, driven at 2.5 Gb/s using the 2^7–1 PRBS. We should note here, that in all cases, (see Sections II-A–II-C), SOAs are operating in the quasi-linear regime, on the edge of weak saturation regime where no patterning problems arise due to a larger number of consecutive identical bits [24]. At the symbol rates under consideration with seven consecutive ones and six consecutive zeros provided by a 2^7–1 PRBS, we capture the bulk of SGM and one should not expect much degradation for longer sequences of consecutive ones and zeros due to SGM/XGM. Thermal effects in SOAs are slow (on the order of MHz) and should not affect symbols along the duration of the OSMOSIS packet (≅51.2 ns at 40 Gb/s). The optical signal at the output of the quadrature modulator is amplified by a second flat-gain EDFA and is polarization division multiplexed (PDM). Similar to Fig. 1, the wavelength selection at each receiver is performed by three tunable filters in tandem, used for fiber, waveband, and wavelength selection, respectively, as described in Section II-A. It is worth noting that we do not fully exploit the inherent tunability of the coherent receiver, which allows for wavelength selection by simply adjusting the current of the LO. We maintain the three selection stages before the coherent receiver in order to study the impact of distortions induced by SOA concatenation on PDM-QPSK and perform a fair comparison with IM/DD and NRZ-DPSK. After the last selection stage, we perform ASE noise loading, the signal is filtered by a last AWG DMUX, acting as a Gaussian optical bandpass filter (OBPF) with 0.8-nm 3-dB bandwidth, and detected by a polarization- and phase-diversity coherent receiver. The LO is a 200-kHz 3-dB linewidth ECL. The photocurrents at the output of the photodetectors are sampled using a real-time digital oscilloscope operating at 5 GSamples/s. The samples are then stored and processed offline [35]. The available SOAs that were used had a PDG <0.2 dB. SOAs with higher PDG were not investigated in the context of this study. The DSP in the coherent receiver could potentially compensate for the PDG since it incorporates an adaptive equalizer based on the constant modulus algorithm (CMA) for polarization demultiplexing and equalization of polarization-multiplexed optical signals. The CMA equalizer, indeed, compensates for the unequal power levels of the two polarization components due to PDG through the CMA operation. Besides, it should be noted that recent progress in photonic technology already allows to fabricate polarization-insensitive SOAs for a wide range of integration platforms, such as monolithic InP of silicon-on-insulator platforms that heterointegrate InP gain blocks.

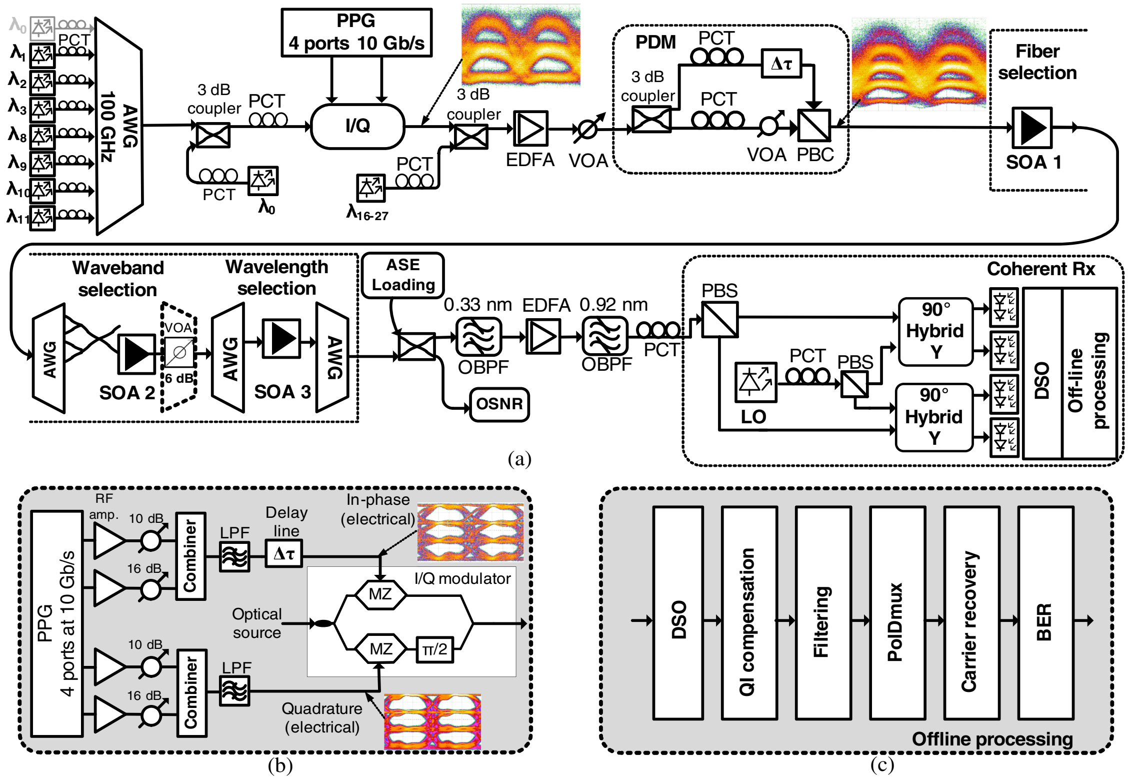

Fig. 5. (a) Experimental setup for the investigation of the transmission performance of 40-Gb/s SP-16QAM and 80-Gb/s PDM-16QAM in the optimized 64 × 64 OSMOSIS optical interconnect architecture. (b) 16-QAM transmitter configuration. (c) DSP algorithms. (Symbols: PCT = polarization controller, AWG = arrayed waveguide gratings, PPG = pattern pulse generator, I/Q = quadrature modulator, EDFA = erbium-doped fiber amplifier, VOA = variable optical attenuator, PDM = polarization division multiplexing, PBC = polarization beam combiner, SOA = semiconductor optical amplifier, ASE = amplified spontaneous emission, OSNR = optical signal-to-noise ratio, OBPF = optical bandpass filter, LO = local oscillator, PBS = polarization beam splitter, DSO = digital sampling oscilloscope, Rx = receiver, QI = quadrature imbalance, PolDmux = polarization demultiplexing, BER = bit error rate).

The BER is measured by error counting as a function of the OSNR for each one of the transmitted wavelengths. BER is also measured as a function of the input power at the first SOA as a metric of PDM-QPSK resilience to SOA nonlinearities.

In principle, we can reduce the cost of the coherent receiver and fully exploit the inherent tunability of the coherent receiver by eliminating the LO laser, as shown in Fig. 4. In Fig. 4, the output power of each laser source is split into two components. One of them is PDM-QPSK modulated and is broadcasted to all the receivers using a $N \times N$ coupler, while the second power component enters the OSMOSIS 64 × 64 optical interconnect architecture. The desired LO wavelength is selected using three SOA-based wavelength selective stages, as described in [17]–[18].

C. SP- and PDM-16QAM Experimental Setup

The experimental setup for the investigation of the transmission performance of SP- and PDM-16QAM modulation format through the OSMOSIS 64 × 64 optical interconnect architecture is shown in Fig. 5(a). The wavelength allocation scheme is the same as in Fig. 2, i.e., $\lambda_0 = 1546.897$ nm and the channel spacing within a waveband is $\Delta f = 100$ GHz. Similar to Section II-B, the performance of each channel is measured after substituting the transmitter DFB laser by an ECL (although, in this case, given the strict linewidth requirements of 16-QAM, we used a better ECL with a 100 kHz 3-dB linewidth).

In Fig. 5(a), seven laser sources (e.g., λ_1–λ_{11}) are multiplexed by a 100-GHz AWG MUX, and are subsequently combined with the wavelength under test (e.g., λ_0), through a 3 dB coupler. Then, the WDM signal enters the quadrature (I/Q) modulator. The in-phase and quadrature components of the electric field of the optical wave are modulated by four-level electrical waveforms provided by a pulse pattern generator (PPG) operating at a symbol rate of 10 Gb/s. The experimental implementation of the transmitter is shown in detail in Fig 5(b). Four electrical PRBSs of period $2^{15}-1$, which are generated by a PPG operating at a clock frequency of 10 GHz, are amplified by four identical microwave amplifiers. Each pair is subsequently attenuated by 10 and 16 dB, respectively. The four binary signals are properly combined in pairs by microwave combiners and the two outputs of the combiners are low-pass filtered. One of the quaternary signals is delayed with respect to the other by one symbol period, using an electrical delay line, so that the two quadrature components are completely decorrelated and synchronized. The resulting direct detection eye diagrams of the quaternary waveforms are shown in the inset of Fig. 5(b). The direct detection eye diagram of the generated 40-Gb/s SP-16QAM output optical signal is shown in the inset of Fig. 5(a), where we can distinguish the three intensity levels that correspond to the three concentric circles of the square

16QAM constellation [36]. Next, a ninth CW laser source with eight times the power of an individual channel and wavelength in the $\lambda_{21.5}$ slot (see Fig. 2), is added to the eight modulated signals, in order to emulate the remaining two wavebands shown in Fig. 2. Subsequently, the WDM signal is boosted by an EDFA in order to compensate for the losses in the modulator and in the couplers. Afterward, the WDM signal is attenuated by 18 dB by using a VOA that emulates the 1:64 power splitting losses present in actual OSMOSIS 64 $\times$ 64 switch fabric due to the broadcasting of the WDM signal to all 64 receiver cards [16]. In Fig. 5(a), the PDM stage is omitted for the SP-16QAM experiment but is included for the generation of the 80 Gb/s PDM-16QAM signals. The direct detection PDM-QPSK eye diagram is shown in the inset of Fig. 5(a) [36]. Next, the signal enters the emulated 64 $\times$ 64 OSMOSIS switch fabric, which consists of three selection stages, i.e., the fiber, the waveband, and the wavelength selection stage, similar to Figs. 1 and 3. At the receiver, ASE noise is loaded to the signal by a 3 dB coupler after the last selection stage, in order to vary the received OSNR. A 0.33-nm 3-dB bandwidth OBPF is used to filter out the wavelength under test, which is then preamplified and filtered again by a 0.92-nm 3-dB OBPF to remove out-of-band ASE noise. The signal is detected by a polarization- and phase-diversity coherent receiver. The LO used in the experiment is an ECL with 100 kHz 3-dB linewidth. The outputs of photodetectors are sampled using a real-time digital oscilloscope and the stored data are processed offline using the DSP algorithms shown in Fig. 5(c) [37]. First, the received signal is passed through a filter approximating a matched filter to increase signal-to-noise ratio. Next, any potential I/Q imbalance is compensated [38] and the signal is resampled to two samples/symbol followed by amplitude normalization. Polarization demultiplexing and equalization is performed using a lattice adaptive filter in a butterfly configuration whose taps are updated using the CMA [39]–[40]. Once filters converge, a decision-directed carrier recovery is used to remove the frequency offset due to nonzero intermediate frequency offset between received signal and LO laser [38]. Finally, digital demodulation is performed and BER is calculated by comparing the obtained bit sequence with the known transmitted PRBS of length $2^{15}-1$. BER as a function of the input power in the first SOA is also measured, as previously, for SP-16QAM, to test the resilience in SOA nonlinearities.

III. Results and Discussion

A. 10-Gb/s NRZ-DPSK

In this section, we present the results for the experimental study described in Section II-A. BER measurements as a function of the OSNR are performed in the following cases: i) back-to-back, i.e., when the selection stages of the OSMOSIS 64 $\times$ 64 optical switch fabric in Fig. 1 are omitted; and ii) after transmission through the OSMOSIS 64 $\times$ 64 optical switch fabric. The results are shown in Fig. 6.

The performance of all DPSK implemented channels is approximately the same, i.e., OSNR spread of the curves is around 1 dB at BER $= 10^{-3}$. No significant penalty is observed between the back-to-back case and the best channel (λ_8), while a 1-dB OSNR penalty is measured for the worst channel (λ_0).

To test the robustness of NRZ-DPSK to SOA nonlinearities in the OSMOSIS 64 $\times$ 64 interconnect architecture, the Q-factor is estimated using the measured BER for channel λ_0 at various launch powers into the first SOA of Fig. 1. The results are shown in Fig. 7 (black squares) and are compared with the corresponding measurements for IM/DD (red circles). The experimental setup used for the study of IM/DD is described in detail in [10]. Taking as an arbitrary reference $Q = 11$ dB (corresponding to BER $\cong 2 \times 10^{-4}$), DPSK proves to outperform IM/DD by 9 dB in terms of the dynamic range of the received signal. As dynamic range, we define the power range at the input of the first SOA for which the Q-factor remains above 11 dB. Discontinuities in the DPSK black curve correspond to error-free transmission at these input power values.

To illustrate the impact of concatenated SOAs on the performance of DPSK, representative eye diagrams are shown in Fig. 8(i)–(iii) after the fiber, the waveband and the wavelength selection stage of the OSMOSIS 64 $\times$ 64 switch architecture, respectively, for the worst channel. We observe that the eye opening does not degrade significantly as the number of the selection stages increases. In conclusion, DPSK is more resilient to SOA nonlinearities [19] than conventional IM/DD due to its envelope constancy [32] and constitutes a possible candidate for the next-generation optical interconnects to replace IM/DD.

B. 10-Gb/s Coherent NRZ PDM-QPSK

In this section, the results for the experimental setup described in Section II-B are presented. Fig. 9 shows different sets of BER curves versus OSNR. The rightmost set consists of experimental measurements, for the best and the worst channels, when employing IM/DD [blue curves with circles and crosses, respectively, denoted as (i)]. These results are obtained using the experimental setup presented in [10]. Next to the left, experimental results are shown for each one of the eight implemented coherent PDM-QPSK channels [set (ii)], obtained using the experimental setup described in Section II-B. More specifically, results for the back-to-back configuration (dashed line with black squares), as well as after transmission through the optical interconnect (various symbols), are shown. Black solid lines with circles and crosses in set (ii) represent the best and the worst channel performance after transmission, respectively. All other channels are represented by different symbols falling in between the aforementioned extreme cases. We observe that coherent PDM-QPSK outperforms IM/DD by approximately 3 dB at BER $= 10^{-3}$ when transmitted through the three-stage optimized interconnect architecture. The OSNR penalties at BER $= 10^{-3}$ for the PDM-QPSK best and worst channels are 0.5 and 1 dB, respectively, compared to the back-to-back case [black brokenline in set (ii)]. The remaining curves of Fig. 9 are described later in that Section.

The measured BER performance, for both X and Y polarization tributaries for each PDM-QPSK channel under test, is shown in Fig. 10 (crosses and squares, respectively). Results reveal that both polarization tributaries perform almost the same for all eight wavelengths.

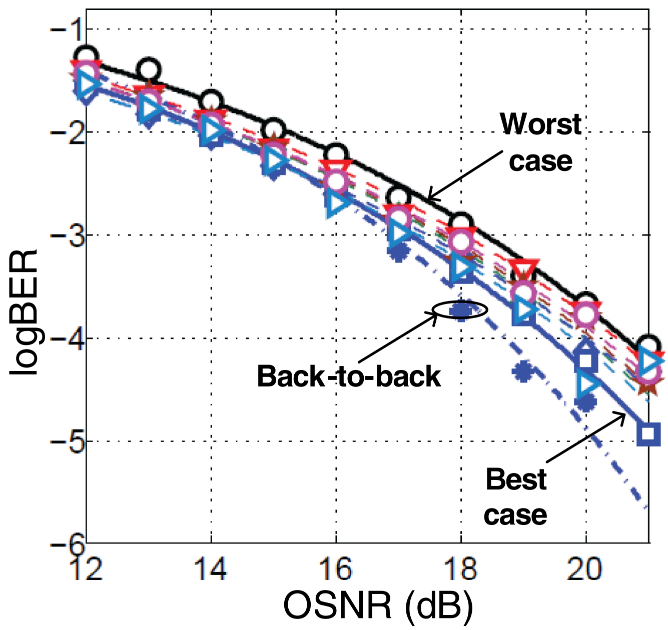

Fig. 6. BER versus OSNR (measured in 0.1-nm resolution bandwidth) for the eight implemented wavelengths. Experimental data are fitted with exponential curves.

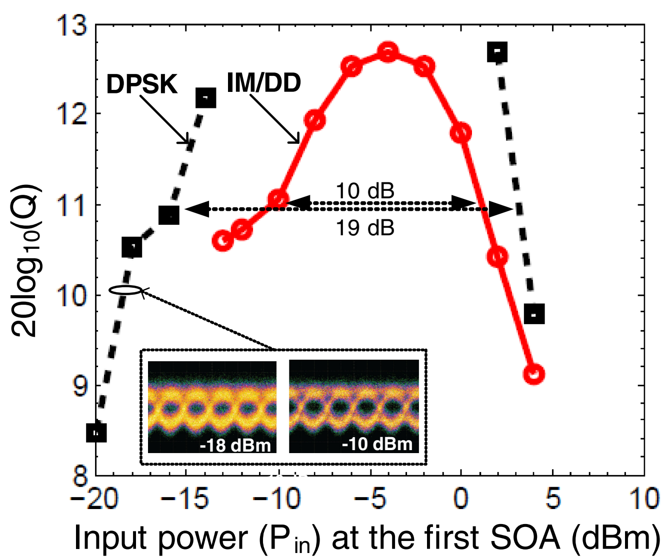

Fig. 7. Q-factor versus launch power in the first SOA for 10-Gb/s DPSK and 10-Gb/s IM/DD. Eye diagrams for $P_{\rm in} = -10$ dBm and –18 dBm for the DPSK case are shown in the inset.

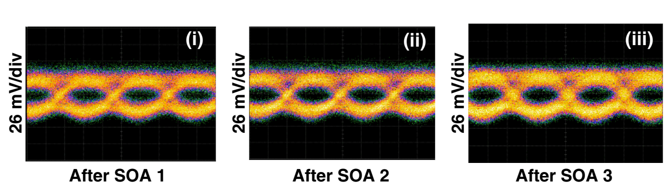

Fig. 8. Measured NRZ-DPSK eye diagrams for the worst channel after each consecutive selection stage of the optimized OSMOSIS 64 × 64 optical switch fabric architecture.

Representative PDM-QPSK constellation diagrams at the output of the coherent receiver are shown in Fig. 9 (inset) and Fig. 11(a) for the back-to-back case and after transmission through three SOA-based selective stages, respectively. The gradual azimuthal elongation of the QPSK constellation points from Fig. 9 (inset) to Fig. 11(a) is attributed to SOA self-phase modulation (SPM) and XPM. Nevertheless, the resulting performance degradation due to transmission effects is still affordable when the total launch power in the first SOA is $P_{\rm in} = -4$ dBm [10].

Returning to Fig. 9, the coherent PDM-QPSK measurements are compared to simulation results [set of curves denoted by (iii)]. The simulation parameters are not optimal but are chosen in order to replicate the specific experimental conditions. For instance, the RF drive voltages of the quadrature modulator are 75% of the half-wave voltages, due to lack of adequate microwave driver amplifiers in the experiment. The back-to-back case (black crosses), the single-channel case (green solid line), and the WDM case (green circles and crosses, for the best and the worst case channels, respectively) are collectively shown in set (iii). There is a spread of $\sim$1 dB in the simulated curves, similar to the experiment. On the other hand, the back-to-back, the single-channel, and the WDM best channel curves coincide. We also observe that the experimental measurements are worse than the simulation results by approximately 0.8 dB at BER $= 10^{-3}$. This implementation penalty is attributed to different component imperfections of the experimental setup, which are not taken into account in the simulations.

Next, we test the vulnerability of the two formats to SOA nonlinearities by varying the input power into the first SOA of the 64 × 64 optical switch fabric. Results are shown in Fig. 11(c), both for PDM-QPSK and for IM/DD (using the experimental setup of [10]), for the same OSNR = 11 dB. We observe that IM/DD (◯) performs better at low input powers (<–12 dBm) since the slope of the curve is smaller than in the PDM-QPSK case (□) for the same range of values. The added ASE noise from the unsaturated SOA is the dominant factor of degradation in this regime for PDM-QPSK. At higher input powers, PDM-QPSK is proven to be more tolerant to SOA nonlinearities exhibiting a smaller Q-factor slope than IM/DD. PDM-QPSK outperforms IM/DD in terms of dynamic range, defined in this case as the power range at the input of the first SOA for which the BER remains below the FEC limit (i.e., below $20\log_{10}(\mathrm{Q}) = 7.3$ dBQ corresponding to a BER of 10^{-2}, when using advanced coding [42]). The dynamic range is 13 and 6 dB for PDM-QPSK and IM/DD, respectively. Constellation diagrams for PDM-QPSK and eye diagrams for IM/DD transmission after transmission through the OSMOSIS 64 × 64 optical interconnect are shown in Fig. 11(a) and (b), for input powers to the first SOA equal to -4 dBm (entering the saturation regime) and to 2 dBm (in saturation regime), respectively. At high input powers, SOAs induce nonlinear phase noise distortion, which is the dominant reason for PDM-QPSK performance degradation as it is evident from the constellations of Fig. 11(a) and (b). More specifically, comparing Fig. 11(a) to Fig. 11(b), we observe that the azimuthal elongation of the constellations is a tell-tale sign of SMP/XPM, while IM/DD eye diagrams are primarily vulnerable to SGM/XGM.

For comparison, we evaluated, by simulation, the performance of the alternative optical interconnect shown in Fig. 4.

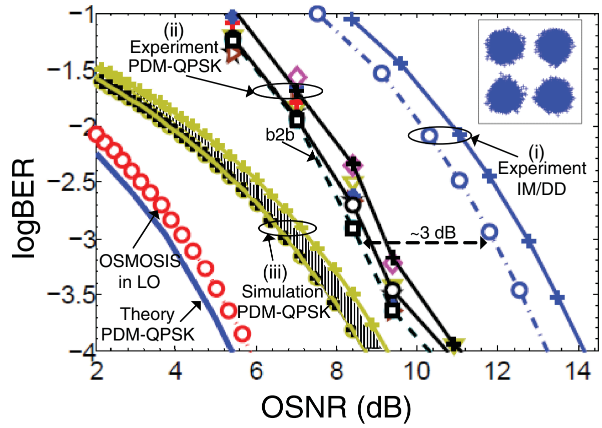

Fig. 9. BER versus OSNR. (i) Experimental measurements for the best and the worst case transmission scenario for IM/DD presented in [10]. (ii) Experimental measurements for all PDM-QPSK channels. (iii) Simulation results for realistic experimental conditions, i.e., when the RF driving voltages of the QPSK modulator are 75% of the ideal values. Red open circles (simulation): BER versus OSNR for λ_1 of the configuration of Fig. 4 in the 64 × 64 case. Blue solid line: Theoretical curve for the back-to-back case using a semianalytical method for the error probability evaluation of PDM-QPSK [41]. Inset: Constellation diagram for PDM-QPSK for the back-to-back case for OSNR = 11 dB.

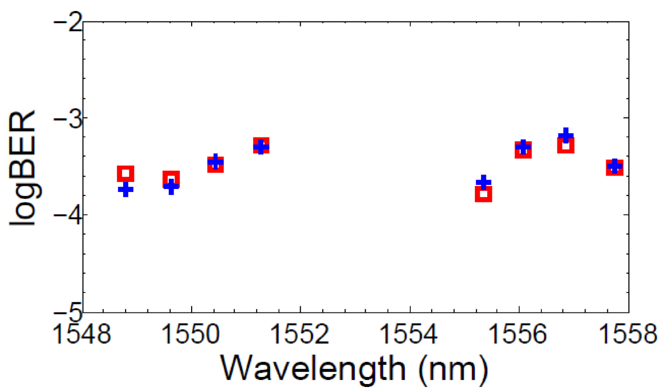

Fig. 10. Measured BER of the eight implemented channels for coherent PDM-QPSK after the three selection stages at the receiver. (Symbols: Squares: X polarization tributary, Crosses: Y polarization tributary).

The BER versus OSNR curve for λ_1 is shown in Fig. 9 (red curve with open circles denoted as "OSMOSIS in LO"). The penalty in that case, after transmission, is less than 1 dB compared to the theoretical curve. This is due to the fact that, in this alternative configuration, it is possible to avoid nonlinear effects, such as SPM and XPM, because the WDM data signal does not pass through any SOAs. Moreover, self-homodyne detection almost completely eliminates the phase noise in the system, if the optical path lenghts of the signal and the LO branches are matched.

C. Coherent 40-Gb/s SP-16QAM and 80-Gb/s PDM-16QAM

In this section, the results for the experimental setup described in Section II-C are presented. BER versus OSNR measurements are carried out for λ_3 after each selection stage using the experimental setup of Fig. 5(a), for 40-Gb/s SP-16QAM. The results are shown in Fig. 12. Taking as a reference for the FEC limit a BER $= 10^{-3}$, we observe that the penalty between the first and the second selection stage is less than 0.5 dB, in terms of

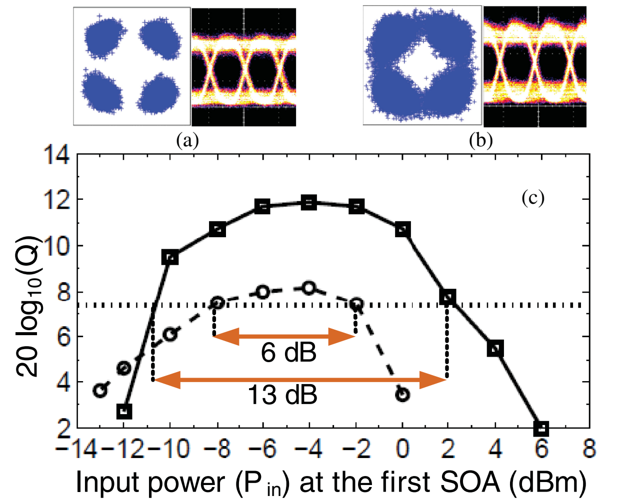

Fig. 11. (a) and (b) Constellation diagrams for PDM-QPSK and eye diagrams for IM/DD after transmission through the OSMOSIS 64 × 64 optical interconnect, for launch powers to the first SOA in Fig. 3 equal to –4 and 2 dBm, respectively. (c) Measured Q-factor for λ_0 versus launch power to the first SOA in Fig. 3 for PDM-QPSK (□) and IM/DD (◯). (Conditions: OSNR = 11 dB).

required OSNR, while there is no penalty between the second and the third selection stage. Error floors in the performance arise for all three cases, being more pronounced after the third selection stage, indicating that the nonlinearities imposed by SOAs set a limit on the scalability of the interconnect.

Fig. 13 compares the BER versus the OSNR for the SP-16QAM (crosses) and PDM-16-QAM (circles) case, after transmission through the OSMOSIS interconnect for λ_3. The results for 10 Gb/s IM/DD were reported in [10] but are shown also here as a reference (squares). SP- and PDM-16QAM, increase the capacity by a factor of 4 and 8, respectively, using the same 10-GBd equipment as IM/DD, at the expense of 4 and 8 dB penalty in required OSNR at BER $= 10^{-3}$, respectively. The penalty for 80-Gb/s PDM-16QAM compared to 40-Gb/s SP-16QAM is around 4 dB at BER $= 10^{-3}$. A 3 dB penalty is expected from theory [32]. This implies that polarization crosstalk induces an additional 1 dB performance penalty when PDM-16QAM is employed. Error floors in BER performance occur for both PDM-16-QAM and SP-16QAM. Nevertheless, BER is well below the FEC limit, i.e., BER $= 10^{-3}$ in both cases.

In Fig. 14, the measured BER performance, for each one of the eight 16QAM modulated channels, is shown for the SP and the PDM case, with squares and circles, respectively, for the same OSNR = 23 dB. In the SP-16QAM experiment, all eight measured channels exhibit approximately the same BER for the same OSNR = 23 dB. On the other hand, the BER variation among channels in the PDM-16QAM case is larger. Representative constellation diagrams are shown on the right of Fig. 14, for the worst channel, for both the SP-16QAM and the PDM-16QAM.

Finally, the Q-factor versus the first SOA input power for all modulation formats that are investigated in the 64 × 64 optical interconnect, in this paper, is shown for 10-Gb/s DPSK (squares), 10-Gb/s PDM-QPSK (diamonds), and 40-Gb/s SP-QAM (circles) in Fig. 15. First of all, we observe that the Q-factor dependence from the launch power P in the first SOA for coherent optical communications systems can be described well by the empirical relationship (1) later, which is arbitrarily adopted from the formalism [43]–[46] describing the scaling of fiber-induced nonlinearities with the launch power

$$\hat{Q}^2 = \frac{P}{a + \beta P + \gamma P^3} \tag{1}$$

where the coefficients a, β, γ are determined by fitting (see Fig. 16).

From Fig. 15, we observe that NRZ-DPSK is more tolerant to SOA nonlinearities than SP-16QAM, as it allows for error free operation (above a hypothetical FEC limit of $Q = 10$ dB) for a power range of 20 dB input power, for the same OSNR. On the other hand, coherent PDM-QPSK has a smaller dynamic range of 10 dB at $Q = 10$ dB, since it is more vulnerable to the phase noise induced by the SOAs. Performance is degraded rapidly as the input power increases. Particularly, we can discriminate between the OSNR-limited, and the nonlinearities-limited dynamic power range, for the left and the right slope of the Q-factor curve, respectively, as the difference in SOA input power between the maximum Q and $Q_{3\mathrm{dB}}$ ($Q_{3\mathrm{dB}}$ is the Q-value for which the Q-factor shows a 3 dB penalty with respect to its maximum), on both sides of the curve. More specifically, for 10-Gb/s PDM-QPSK OSNR-limited range is 6 dB and nonlinearities-limited range is 4 dB, and for 40-Gb/s SP-16QAM OSNR-limited range is 3 dB and nonlinearities-limited range is 6 dB. So, coherent PDM-QPSK has a larger OSNR-limited dynamic range and a narrower nonlinearities-limited one. Finally, SP-16QAM with coherent detection has an even narrower total dynamic range of 9 dB at $Q = 10$ dB, exhibiting the worst performance, since it is even more sensitive to phase noise due to its denser constellation structure. Representative constellation diagrams are shown in Fig. 17(a)–(d) for SP-16QAM, for input powers -21, 17, -11, and -9 dBm, respectively. The shape of the constellation points reveals that the signal degradation is due to phase nonlinearities that become critical at high input powers and set a limit to the performance of the interconnect [see Fig 17(c) and (d)].

Comparing the dynamic range of the curves shown in Fig. 15, for the optimized 64 × 64 OSMOSIS interconnect architecture, to the one presented in [16], for the original 64 × 64 OSMOSIS architecture, at $Q_{3\mathrm{dB}}$, it is shown that the performance of the optimized architecture is significantly degraded for the OSNR-limited range (>15 dB), while, on the other hand, the degradation in the nonlinearities-limited dynamic range is much less for PDM-QPSK and 16QAM (in the order of ∼4 and ∼2 dB, respectively). This reveals once again that the latter formats are more vulnerable to ASE noise, as well as to phase noise nonlinearities, both induced by the SOAs. The impact of these effects becomes more pronounced in the optimized 64 × 64 OSMOSIS interconnect architecture, as it uses one more SOA at each receiver card, thus exacerbating the nonlinear effects.

The use of alternative DSP algorithms [47]–[48] to counteract the SOA-induced nonlinear effects could potentially improve the overall performance of the advanced modulation formats under investigation in this paper. Alternatively, several DSP algorithms have been proposed that reduce the phase noise induced by fiber nonlinearities. Variants of the Viterbi–Viterbi blind feedforward carrier phase estimation algorithm like the one presented in [49],

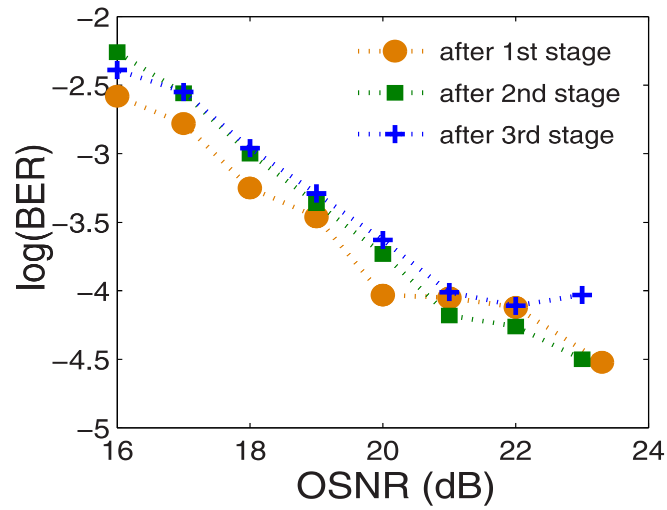

Fig. 12. BER versus OSNR for λ_3 after the first (circles), the second (squares) and the third (crosses) selection stage of the OSMOSIS 64 × 64 optimized switch architecture using 40 Gb/s SP-16QAM.

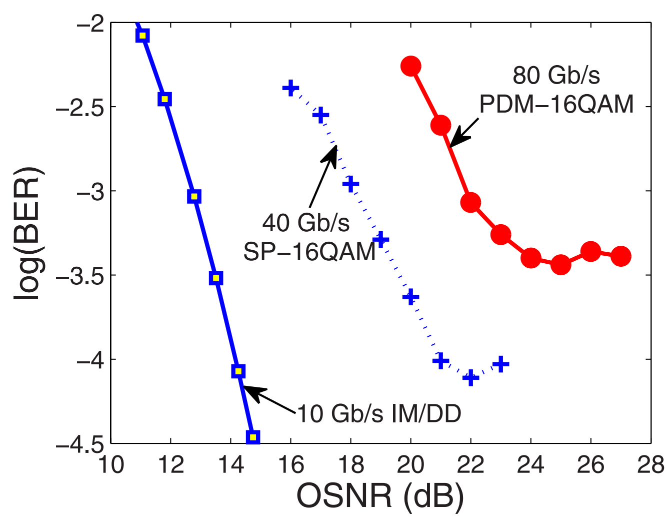

Fig. 13. BER versus OSNR for 10-Gb/s IM/DD (squares) [10], 40-Gb/s SP-16QAM (crosses), and 80-Gb/s PDM-16QAM (circles).

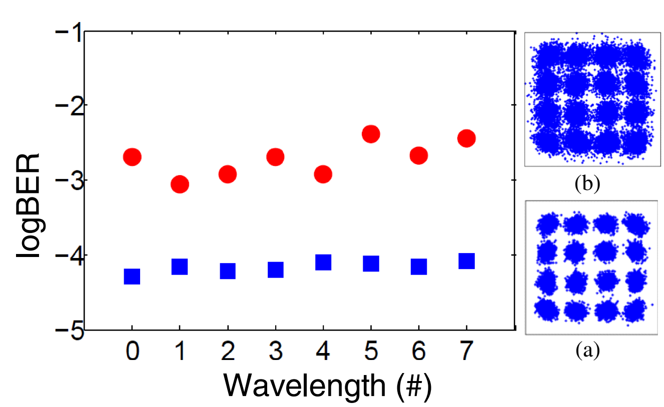

Fig. 14. BER performance for all implemented channels for SP-16-QAM (squares) and PDM-16-QAM (circles) at OSNR = 23 dB. Representative constellation diagrams for the worst (a) SP-16-QAM and (b) PDM-16-QAM channels are shown on the right.

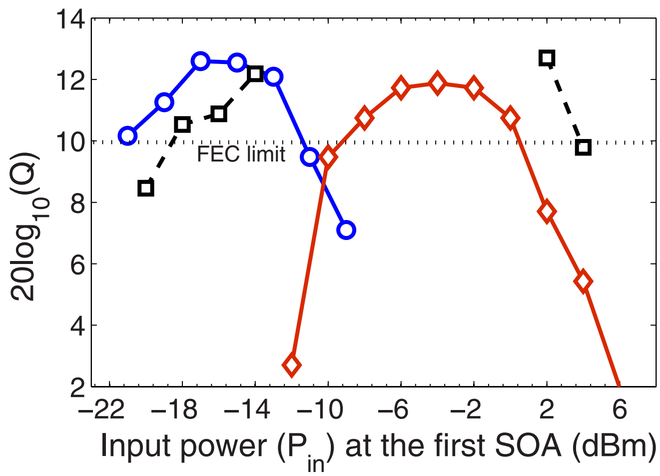

Fig. 15. Q-factor versus launch powers to the first SOA for 10-Gb/s NRZ-DPSK (squares), 10-Gb/s PDM-QPSK (diamonds), and 40-Gb/s SP-16QAM (circles) modulation formats.

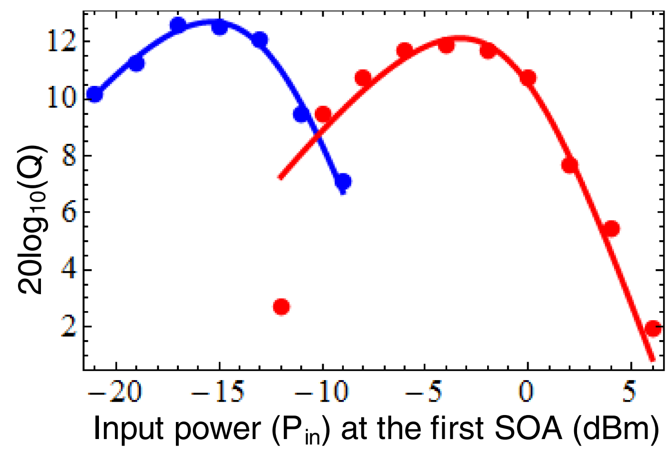

Fig. 16 Q-factor versus launch power to the first SOA for 10-Gb/s PDM-QPSK (in red) and 40-Gb/s SP-16-QAM (in blue). [Symbols: points: measurements, solid lines: least squares fit by (1)]. (Fitting parameters: For SP-16 QAM: $\alpha = 0.000569542$ mW, $\beta = 0.0242352$ mW^{-1}, $\gamma = 11.5402$ mW^{-2}; For PDM QPSK: $\alpha = 0.00998607$ mW, $\beta = 0.0288942$ mW^{-1}, $\gamma = 0.049598$ mW^{-2}).

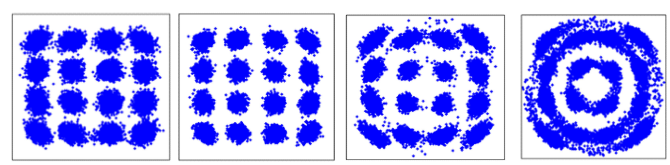

Fig. 17. Constellation diagrams for SP-16QAM corresponding to (a) –21 dBm; (b) –17 dBm; (c) –11 dBm; and (d) –9 dBm launch power in the first SOA of the optimized OSMOSIS 64 × 64 optical interconnect architecture.

customized for SOAs, could be used for compensating phase noise from SOA-induced nonlinearities. One could envision the use of these algorithms for SOA-induced nonlinear phase noise.

Finally, we should note that another alternative potential candidate advanced modulation format, such as OFDM-QPSK, has been also investigated in a simplified version of the 64 × 64 OSMOSIS optical interconnect architecture [50]. Moreover, carrierless amplitude/phase modulation [51]–[52] could be also considered for future research in the aforementioned optical switch fabric.

IV. System Complexity, Energy Efficiency, and Further Performance Aspects

The technology that will be adopted in the next-generation's HPC interconnects will highly depend on the cost and power consumption of the components that will be employed. Table I summarizes the main contributors in cost and power consumption of the OSMOSIS interconnect architecture for each modulation format under study in this paper.

A. Cost

DPSK would be a favorable solution in terms of cost, as it makes use of the same 3-dB bandwidth components as IM/DD for the same data rate, while at the same time it achieves a 3 dB higher sensitivity [32]. The required phase modulator and balanced receiver increase slightly the cost in that case (see Table I). The deployment of PDM-QPSK, SP-16QAM, and PDM-16QAM with coherent detection in optical interconnects is currently hindered by the prohibitive cost of the coherent transceiver equipment. The strict linewidth requirements of the transmitter laser, employed in those cases, further increase the cost of the architecture, as more expensive ECL lasers need to be employed. Finally, the cost increases further due to the need of either four or eight high-speed microwave driver amplifiers.

Photonic integration will be a key enabling technology in order to employ the presented architecture in such a cost-sensitive segment such as datacom, as it will serve to avoid bulky and costly microoptic assemblies. First of all, it is expected that the cost of photonic integration circuits increases just marginally when moving from a simple modulation format such as IM/DD to a more complex one, since yield and integration density of such circuits are already high enough to effectively integrate larger subsystems such as multichannel optical transmitters or receivers [55]. In the same direction, structures such as QAM modulators with high electrooptical bandwidth of 40 GHz and low required V_π voltage have been recently demonstrated in InP platform [56]. Furthermore, optical sources, such as narrow-linewidth DFB lasers or VCSELs, can benefit from novel cost-effective processes such as nanoimprint lithography [57]. Moreover, avalanche photodetectors with high >300 GHz gain-bandwidth product and compatible with silicon platforms can be realized in SiGe [58], which allows to further decrease the cost/bit when moving to higher bandwidths (i.e., symbol rates) while providing higher compatible loss budgets without extra cost. Most important will be the heterointegration of III–V gain blocks with group IV circuits. Photonics technology is nowadays ready to integrate entire building blocks through cointegration of passive optics (e.g., AWGs), active optical gain components (i.e., SOAs) and electronics [59]–[61]. This enables to implement subsystems onto a single chip, which greatly reduces the number of required fiber couplings, which are the dominant factor of subsystem cost due to the need for active submicrometer alignment and packaging processes. Due to the aforementioned reasons, confidence is provided that in near future cost credentials can be offered to viably introduce advanced modulation formats in datacom at just a marginal cost increase.

TABLE I
COMPLEXITY AND POWER CONSUMPTION PER LINK IN THE 64 × 64 OPTIMIZED OSMOSIS SWITCH FABRIC

Reception Method		Direct Detection		Coherent Detection		
Modulation Format		IM	DPSK	PDM-QPSK	SP-16QAM	PDM-16QAM
Data Rate		10 Gb/s	10 Gb/s	10 Gb/s	40 Gb/s	80 Gb/s
Optics	*Source*	*1 DFB +TEC*	*1 DFB +TEC*	*1 ECL +TEC*	*1 ECL +TEC*	*1 ECL +TEC*
	TX Mod.	*1MZM*	*1 MZM*	*2× I/Q*	*1× I/Q*	*2× I/Q*
	RX Detector	*1 PIN*	*2 PIN (balanced)*	*1 LO, Hybrid 4 PIN*	*1 LO, Hybrid 4 PIN*	*1 LO, Hybrid 4 PIN*
Electronics	*TX Drivers, RF Swing, Mod. biases*	*1, $V\pi$, 1 bias*	*1, $2V\pi$, 1 bias*	*4, $4{\times}2V\pi$, 6 biases*	*4, $2{\times}2V\pi$, $2{\times}V\pi$ 3 biases*	*8, $4\times 2V\pi$, $4{\times}V\pi$ 6 biases*
	Receivers	*1 TIA*	*2 TIA*	*4 TIA, 4 ADCs (~50 pJ/b per ADC for 20 GS/s [53]–[54]) DSP ASIC*		
Interconnect architecture		*EDFA boosters (+TEC), SOA-based switch (+TEC), environmental conditioning of data center (50% overhead)*				
Per-link energy consumption		*740 pJ/b*	*810 pJ/b*	*1910 pJ/b*	*2350 pJ/b*	*1330 pJ/b*

B. Power Consumption

The main contributors in power consumption for each modulation format are also summarized in Table I. As we can observe, the power consumption slightly increases after substitution of IM/DD by DPSK, for the same data rate, while more sophisticated modulation formats, such as the PDM-QPSK, SP-16QAM, and PDM-16QAM with coherent detection, increase both the transceiver complexity and the electronic power consumption [62]. More specifically, for multilevel modulation formats such as PDM-QPSK, SP- and PDM-16QAM, the transmitter becomes more complex as one or two I/Q modulators are needed for the SP or PDM schemes, respectively. Further increase in energy consumption is due to the deployment of either four or eight high-speed microwave driver amplifiers. It is worth noting that the energy consumption of coherent systems is dominated by the transceiver electronics and in particular the four analog-to-digital converters (ADCs) at the coherent receiver prior to the DSP chip ($\sim$1 W for 20 GS/s per ADC, or 50 pJ/b [53]). In addition, the electronic drivers of the quadrature modulator at the transmitter consume several pJ/b (e.g., the electrical energy consumption is $\sim$25 pJ/b for a driver amplifier operating at 40 Gb/s [63]). Finally, the DSP ASIC, consume several pJ/b each. This is way above 5 pJ/b, which is the current target for commercial optical interconnects.

The power consumption of the 64 × 64 interconnect system is calculated to derive the end-to-end power consumption, shown in the last raw of Table I. For this comparison, a component-level calculation is performed, taking into account the actual transmitter and receiver configuration as it is implemented in the experimental laboratory setups, for 10 Gb/s. The overall power consumption is estimated after the summation of the power consumption of each optical and RF component. Then, it is divided by the number of links, i.e., 64, to get the per-link power consumption, and by the delivered data rate to provide the commonly used per-bit notation. Note that Table I presents the results of an analysis that is based on characteristics of commercial off-the-shelf components rather than relying on values from very recent research results of novel device realizations.

The power consumption of the system could improve in the very optimal case that SOAs, lasers, and EDFAs that are used are uncooled. Further lowering of power consumption could be achieved exploiting the advances in photonic technology, especially with respect to the semiconductor design, i.e., the uncooled operation with GaAs devices. For example, low drive modulators (such as InP I/Q modulators) or efficient light sources (such as VCSELs). Finally, both the CAPEX and the OPEX of coherent optical communications systems must be greatly improved before this technology can be considered as viable alternative for optical interconnects market.

C. Latency

For the original OSMOSIS interconnect architecture, a 10^{-21} BER is achieved after FEC, 75% of the packet length is available for user payload, and the maximum allowable latency is less than 1-ms measured application–application. In addition, FEC techniques that operate efficiently on a packet-by-packet basis are required. Finally, the packet size is fixed at 256 B at a line rate of 40 Gb/s, resulting in a time slot of 51.2 ns [16].

In OSMOSIS interconnect, customized, per packet FEC codes with appropriate overhead that bring the raw BER from $\sim 10^{-4}$ to the required 10^{-21}, while satisfying the initial requirement that 75% of transmitted data per packet must be user information, are required [64]. Reed solomon (RS) codes, e.g., RS (160,128), could satisfy these requirements. Note that in the original OSMOSIS design, the total coding overhead was less than 10%. Latency bottlenecks in the OSMOSIS design arise not from the time of flight of packets through consecutive SOA stages but mainly from contention resolution using an arbiter which computes a one-to-one matching between the inputs and outputs in every time slot. In the OSMOSIS optical switch fabric, this implies that the arbiter should complete about six iterations on a 64 × 64 request matrix in one time slot of 51.2 ns, which is very challenging.

D. Jitter

It is possible to observe static or dynamic timing mismatches between signals going through different optical paths in the OSMOSIS optical switch fabric, such that the resulting optical packets are not synchronized all along the way to the respective receivers. The static timing mismatch between the signal paths may be measured and removed either by using different lengths of fibers in different paths, or, in the case of digital coherent receivers, both static and dynamic mismatches can be removed with the aid of a deskew algorithm [65]. We should point out that there are already very short reach field-programmable gate array implementations for a data rate of 4 × 25 Gb/s taking advantage of clock-data recovery circuits near the optical transceiver blocks in order to reset the jitter budget of the end-to-end data link. Transceivers with very low jitter generation ($<$300 fs rms) have been demonstrated [66]. It is possible to study the impact of jitter on the performance of electronic clock and data recovery circuitry (CDR) at the receiver of active optical cables. There are models describing how the CDR loop responds to data jitter, using either a Markov chain analysis of the loop or by linearizing the loop and treating it as linear control system [67]. Such a study is outside of the scope of this paper.

V. Summary

We investigated the performance of four advanced modulation formats considered for deployment in an optimized 64 × 64 optical interconnect architecture that uses SOAs to perform ns-scale optical switching. We experimentally investigated the performance and proved the superiority of NRZ-DPSK compared to 10-Gb/s IM/DD. NRZ-DPSK is an appealing candidate for the next-generation optical interconnects, due to its low implementation complexity and equipment cost.

We also assessed the performance of coherent 2.5-GBd PDM-QPSK links in the 64 × 64 optical switch fabric. We studied, both theoretically and experimentally, the dynamic range and the robustness to SOA nonlinearities. Our study indicates that coherent PDM-QPSK extends the capacity of the optical switch fabric at the expense of cost and complexity, compared to IM/DD. Nevertheless, it is more vulnerable to phase-noise nonlinearities than NRZ-DPSK. To reduce the cost of the optical interconnect, we can eliminate the LO using the OSMOSIS switch fabric to select the LO wavelength.

Finally, we explored the futuristic scenario of employing SP- and PDM-16QAM in the OSMOSIS 64 × 64 optical interconnect. This implementation further increases the spectral efficiency while still using the same electronic components as 10-Gb/s IM/DD. However, phase-noise-induced nonlinear effects set a limit on the performance of the interconnect.

Acknowledgment

The authors would like to thank Prof. D. Toumpakaris, from the University of Patras, Dr. A. Liveris, from Microwave Networks Inc., and Prof. K. J. Larsen, from the Technical University of Denmark, for fruitful discussions on FEC coding. In addition, the authors are indebted to Dr. B. R. Hemenway and Dr. R. R. Grzysbowski of Corning, Inc., for the donation of several key components and devices used in the experimental setups.

References

[1] P. Pepeljugoski, J. Kash, F. Doany, D. Kuchta, L. Schares, C. Schow, M. Taubenblatt, B. J. Offrein, and A. Benner, "Towards exaflop servers and supercomputers: The roadmap for lower power and higher density optical interconnects," in *Proc. 36th Eur. Conf. Opt. Commun.*, Torino, Italy, Mar. 2010, pp. 1–14, Paper Tu4G3.

[2] P. Pepeljugoski, J. Kash, F. Doany, D. Kuchta, L. Schares, C. Schow, M. Taubenblatt, B. J. Offrein, and A. Benner, "Low power and high density optical interconnects for future supercomputers," in *Proc. Opt. Fiber Commun.*, San Diego, CA, Mar. 2010, pp. 1–3, Paper OThX2.

[3] Y. Benlachtar, R. Bouziane, R. I. Killey, C. R. Berger, P. A. Milder, R. Koutsoyannis, J. C. Hoe, M. Pueschel, and M. Glick, "Optical OFDM for the data center," in *Proc. Int. Conf. Transparent Opt. Netw.*, Munich, Germany, Jun. 2010, pp. 1–4, Paper We.A4.3.

[4] I. H. White, J. D. Ingham, and R. V. Penty, "Systems aspects of optical technologies for use in datacommunications," in *Proc. Opt. Fiber Commun.*, Los Angeles, CA, Mar. 2011, pp. 1–3, Paper OMM1.

[5] P. Milder, R. Bouziane, R. Koutsoyannis, C. R. Berger, Y. Benlachtar, R. I. Killey, M. Glick, and J. C. Hoe, "Design and simulation of 25 Gb/s optical OFDM transceiver ASICs," in *Proc. 37th Eur. Conf. Opt. Commun.*, Geneva, Switzerland, Sep. 2011, pp. 1–3, Paper We9A5.

[6] C. Kachris, E. Giacoumidis, and I. Tomkos, "Energy-efficiency study of optical OFDM in data centers," in *Proc. Opt. Fiber Commun.*, Los Angeles, CA, Mar. 2011, pp. 1–3, Paper JWA87.

[7] K. Szczerba, P. Westbergh, J. Karout, J. Gustavsson, Å. Haglund, M. Karlsson, P. Andrekson, E. Agrell, and A. Larsson, "30 Gbps 4-PAM transmission over 200 m of MMF using an 850 nm VCSEL," *Opt. Exp.*, vol. 12, no. 26, pp. B203–B208, Nov. 2011.

[8] K. Bergman, "Optically interconnected high performance data centers," in *Proc. 36th Eur. Conf. Opt. Commun.*, Torino, Italy, Mar. 2010, pp. 1–3, Paper Mo2D1.

[9] J. Gripp, M. Duelk, J. E. Simsarian, A. Bhardwaj, P. Bernasconi, O. Laznicka, and M. Zirngibl, "Optical switch fabrics for ultra-high-capacity IP routers," *IEEE J. Lightw. Technol.*, vol. 21, no. 11, pp. 2839–2850, Nov. 2003.

[10] F. Karinou, I. Roudas, K. G. Vlachos, B. R. Hemenway, and R. R. Grzybowski, "Influence of transmission impairments on the OSMOSIS HPC optical interconnect architecture," *IEEE J. Lightw. Technol.*, vol. 29, no. 21, pp. 3167–3177, Sep. 2011.

[11] H. Wang, E. T. Aw, M. G. Thompson, A. Wonfor, R. V. Penty, and I. H. White, "High capacity demonstration of a compact regrowth-free integrated 4 × 4 quantum well semiconductor optical amplifier based switch," in *Proc. 34th Eur. Conf. Opt. Commun.*, Brussels, Belgium, Sep. 2008, pp. 1–2, Paper Th1C6.

[12] Y. Kai, K. Sone, S. Yoshida, Y. Aoki, G. Nakagawa, and S. Kinoshita, "A compact and lossless 8 × 8 SOA gate switch subsystem for WDM optical packet interconnections," in *Proc. 34th Eur. Conf. Opt. Commun.*, Brussels, Belgium, Sep. 2008, pp. 1–2, Paper We2D4.

[13] R. P. Luijten and R. Grzybowski, "The OSMOSIS optical packet switch for supercomputers," in *Proc. Opt. Fiber Commun.*, San Diego, CA, Mar. 2009, pp. 1–3, Paper OTuF3.

[14] O. Liboiron-Ladouceur, A. Shacham, B. A. Small, B. G. Lee, H. Wang, C. P. Lai, A. Biberman, and K. Bergman, "The Data Vortex optical packet switched interconnection network," *IEEE J. Lightw. Technol.*, vol. 26, no. 13, pp. 1777–1789, Jul. 2008.

[15] A. Shacham and K. Bergman, "An experimental validation of a wavelength-striped, packet switched, optical interconnection network," *IEEE J. Lightw. Technol.*, vol. 27, no. 7, pp. 841–850, Apr. 2009.

[16] R. Hemenway, R. R. Grzybowski, C. Minkenberg, and R. Luijten, "Optical packet-switched interconnect for supercomputer applications," *J. Opt. Netw.*, vol. 3, no. 11, pp. 900–913, Dec. 2004.

[17] I. Roudas, B. R. Hemenway, and R. R. Grzybowski, "Optimization of a supercomputer optical interconnect architecture," in *Proc. IEEE/OSA LEOS Annu. Meet.*, Lake Buena Vista, FL, Oct. 2007, pp. 741–742, Paper ThG3.

[18] I. Roudas, B. R. Hemenway, R. R. Grzybowski, and F. Karinou, "Optimal wavelength-space crossbar switches for supercomputer optical interconnects," *OSA Opt. Exp.*, vol. 20, pp. 20407–20426, 2012.

[19] R. Ramaswami and P. A. Humblet, "Amplifier induced crosstalk in multichannel optical networks," *IEEE J. Lightw. Technol.*, vol. 15, no. 1, pp. 1882–1896, Jan. 2003.

[20] P. S. Cho, Y. Achiam, G. Levy-Yurista, M. Margalit, Y. Gross, and J. B. Khurgin, "Investigation of SOA nonlinearities on the amplification of DWDM channels with spectral efficiency up to 2.5 b/s/Hz," *IEEE Photon. Technol. Lett.*, vol. 16, no. 3, pp. 918–920, Mar. 2004.

[21] P. S. Cho and J. B. Khurgin, "Suppression of cross-gain modulation in SOA using RZ-DPSK modulation format," *IEEE Photon. Technol. Lett.*, vol. 15, no. 1, pp. 162–164, Jan. 2003.

[22] Z. Li, Y. Dong, J. Mo, Y. Wang, and C. Lu, "1050-km WDM transmission of 8 × 10.709 Gb/s DPSK signal using cascaded in-line semiconductor optical amplifier," *IEEE Photon. Technol. Lett*, vol. 16, no. 7, pp. 1760–1762, Jul. 2004.

[23] Z. Li, Y. Dong, C. Lu, Y. J. Wen, Y. Wang, W. Hu, and T. H. Cheng, "Comparison of cross-gain modulation effect of Manchester-duobinary, RZ-DPSK, NRZ-DPSK, RZ, and NRZ modulation formats in SOAs," *IEEE Photon. Technol. Lett.*, vol. 18, no. 24, pp. 2680–2682, Dec. 2006.

[24] X. Wei, Y. Su, X. Liu, J. Leuthold, and S. Chandrasekhar, "10-Gb/s RZ-DPSK transmitter using a saturated SOA as a power booster and limiting amplifier," *IEEE Photon. Technol. Lett.*, vol. 16, no. 6, pp. 1582–1584, Jun. 2004.

[25] E. Ciaramella, A. D'Errico, R. Proietti, and G. Contestabile, "WDM-POLSK transmission systems by using semiconductor optical amplifiers," *IEEE J. Lightw. Technol.*, vol. 24, no. 11, pp. 4039–4046, Nov. 2006.

[26] F. Karinou, I. Roudas, K. Vlachos, C. S. Petrou, A. Vgenis, and B. R. Hemenway, "Wavelength-space permutation switch with coherent

PDM QPSK transmission for supercomputer optical interconnects," presented at the Optical Fiber Communication Conf. Expo., San Diego, CA, Mar. 2010, Paper JWA62.

[27] F. Karinou, I. Roudas, K. Vlachos, B. R. Hemenway, and R. R. Grzybowski, "Performance assessment of an optimized optical supercomputer interconnect architecture," presented at the Optical Fiber Communication Conf. Expo., San Diego, CA, Mar. 2011, Paper JWA086.

[28] M. P. Fok, C. Shu, and D. J. Blumenthal, "All-Optical ASK-DPSK signal regeneration using a semiconductor optical amplifier," presented at the Conf. Lasers Electro-Optics, Baltimore, MD, May 2007, Paper JTuA126.

[29] N. Kikuchi, K. Sekine, S. Sasaki, and T. Sugawara, "Study on cross-phase modulation (XPM) effect on amplitude and differentially phase-modulated multilevel signals in DWDM transmission," *IEEE Photon. Technol. Lett.*, vol. 17, no. 7, pp. 1549–1551, Jul. 2005.

[30] O. Vassilieva, T. Hoshida, X. Wang, J. Rasmussen, H. Miyata, and T. Naito, "Impact of polarization dependent loss and cross-phase modulation on polarization multiplexed DQPSK signals," presented at the Optical Fiber Communication Conf. Expo., San Diego, CA, Mar. 2008, Paper OThU6.

[31] O. Vassilieva, T. Hoshida, J. C. Rasmussen, and T. Naito, "Symbol rate dependency of XPM-induced phase noise penalty on QPSK-based modulation formats," presented at the 36th European Conf. Optical Communication, Brussels, Belgium, Sep. 2008, Paper We1E4.

[32] R. J. Essiambre, G. Kramer, P. J. Winzer, G. J. Foschini, and B. Goebel, "Capacity limits of optical fiber networks," *IEEE J. Lightw. Technol*, vol. 28, no. 4, pp. 662–701, Feb. 2010.

[33] R. Gutiérrez-Castrejón, L. Schares, and M. Duelk, "SOA nonlinearities in 4×25 Gb/s WDM pre-amplified system for 100-Gb/s Ethernet," *Opt. Quantum Electron*, vol. 40, no. 13, pp. 1005–1019, Mar. 2009.

[34] S. Tanaka, A. Uetake, S. Okumura, M. Ekawa, G. Nakagawa, and K. Morito, "Uncooled, polarization-insensitive AlGalnAs MQW-SOA module operable up to 75°C with constant current," presented at the 37th European Conf. Optical Communication, Geneva, Switzerland, Sep. 2011, Paper Tu.6.LeSaleve.2.

[35] C. S. Petrou, A. Vgenis, I. Roudas, and L. Raptis, "Quadrature imbalance compensation algorithms for coherent PDM QPSK systems," in *Proc. IEEE/OSA LEOS Annu. Meeting*, Belek-Antalya, Turkey, Oct. 2009, pp. 642–643, Paper ThE3.

[36] S. Makovejs, D. S. Millar, D. Lavery, C. Behrens, R. I. Killey, S. J. Savory, and P. Bayvel, "Characterization of long-haul 112Gbit/s PDMQAM-16 transmission with and without digital nonlinearity compensation," *OSA Opt. Exp.*, vol. 18, no. 12, pp. 12939–12947, Jun. 2010.

[37] R. Borkowski, F. Karinou, M. Angelou, V. Arlunno, D. Zibar, D. Klonidis, N. Guerrero Gonzalez, A. Caballero, I. Tomkos, and I. Tafur Monroy, "OSNR requirements in flexgrid optical networks," *OSA/IEEE J. Opt. Com. Netw.*, to be published.

[38] S. J. Savory, "Digital coherent optical receivers: Algorithms and subsystems," *IEEE J. Sel. Topics Quantum Electron.*, vol. 16, no. 5, pp. 1164–1179, Sep./Oct. 2010.

[39] J. R. Treichler and M. G. Larimore, "New processing techniques based on the constant modulus adaptive algorithm," *IEEE Trans. Acoust., Speech, Signal Process.*, vol. ASSP-33, no. 2, pp. 420–431, Apr. 1985.

[40] P. J. Winzer, A. H. Gnauck, C. R. Doerr, M. Magarini, and L. L. Buhl, "Spectrally efficient long-haul optical networking using 112-Gb/s polarization-multiplexed 16-QAM," *IEEE J. Lightw. Technol.*, vol. 28, no. 4, pp. 547–556, Feb. 2010.

[41] M. C. Jeruchim, "Techniques for estimating the bit error rate in the simulation of digital communications systems," *IEEE J. Sel. Areas Commun.*, vol. SAC-2, no. 1, pp. 153–170, Jan. 1984.

[42] T. Mizuochi, Y. Miyata, T. Kobayashi, K. Ouchi, K. Kuno, K. Kubo, K. Shimizu, H. Tagami, H. Yoshida, H. Fujita, M. Akita, and K. Motoshima, "Forward error correction based on block turbo code with 3-bit soft decision for 10-Gb/s optical communication systems," *IEEE J. Sel. Topics Quantum Electron.*, vol. 10, no. 2, pp. 376–386, Mar./Apr. 2004.

[43] P. Poggiolini, A. Carena, V. Curri, G. Bosco, and F. Forghieri, "Analytical modeling of non-linear propagation in uncompensated optical transmission links," *IEEE Photon. Technol. Lett.*, vol. 23, no. 11, pp. 742–744, Jun. 2011.

[44] W. Shieh and X. Chen, "Information spectral efficiency and launch power density limits due to fiber nonlinearity for coherent optical OFDM systems," *IEEE Photon. J.*, vol. 3, no. 2, pp. 158–173, Apr. 2011.

[45] P. Bononi, P. Serena, N. Rossi, E. Grellier, and F. Vacondio, "Modeling nonlinearity in coherent transmissions with dominant intrachannel-four-wave-mixing," *OSA Opt. Exp.*, vol. 20, pp. 7777–7791, Mar. 2012.

[46] A. Carena, V. Curri, G. Bosco, P. Poggiolini, and F. Forghieri, "Modeling of the impact of nonlinear propagation effects in uncompensated optical coherent transmission links," *IEEE J. Lightw. Technol.*, vol. 30, no. 10, pp. 1524–1539, May 2012.

[47] F. Vacondio, A. Ghazisaeidi, A. Bononi, and L.-A. Rusch, "Low-complexity compensation of SOA nonlinearity for single-channel PSK and OOK," *IEEE J. Lightw. Technol.*, vol. 28, no. 3, pp. 277–288, Feb. 2010.

[48] A. Ghazisaeidi and L.A. Rusch, "On the efficiency of digital back-propagation for mitigating SOA-induced nonlinear impairments," *IEEE J. Lightw. Technol.*, vol. 29, no. 21, pp. 3331–3339, Nov. 2011.

[49] Z. Tao, L. Li, L. Liu, W. Yan, H. Nakashima, T. Tanimura, S. Oda, T. Hoshida, and J. C. Rasmussen, "Improvements to digital carrier phase recovery algorithm for high-performance optical coherent receivers," *IEEE J. Sel. Topics Quantum Electron.*, vol. 16, no. 5, pp. 1201–1209, Sep./Oct. 2010.

[50] G. A. Rodes, J. J. Vegas Olmos, F. Karinou, I. Roudas, L. Deng, X. Pang, and I. Tafur Monroy, "Optical switching for dynamic distribution of wireless-over-fiber signals," in *Proc. IEEE 16th Int. Conf. Optical Network Design Modeling*, Essex, U.K., Apr. 2012, pp. 622–627, Paper Wed4P3.

[51] X. Zhou and J. Yu, "Multi-level, multi-dimensional coding for high-speed and high-spectral-efficiency optical transmission," *IEEE J. Lightw. Technol.*, vol. 27, no. 16, pp. 3641–3653, Aug. 2009.

[52] R. Rodes Lopez, M. Wieckowski, J. B. Jensen, J. Turkiewicz, J. Siuzdak, and I. Tafur Monroy, "Carrierless amplitude phase modulation of VCSEL with 4 bit/s/Hz spectral efficiency for use in WDM-PON," *OSA Opt. Exp.*, vol. 19, no. 27, pp. 26551–26556, Dec. 2011.

[53] M. Glick, Y. Benlachtar, and R. I. Killey, "Performance and power consumption of digital signal processing based transceivers for optical interconnect applications," presented at the Int. Conf. Transparent Optical Networks, Azores, Portugal, Jun. 2009, Paper We.B2.3.

[54] R. Bouziane, P. Milder, R. Koutsoyannis, Y. Benlachtar, C. R. Berger, J. C. Hoe, M. Puschel, M. Glick, and R. I. Killey, "Design studies for an ASIC implementation of an optical OFDM transceiver," presented at the European Conf. Optical Communication, Torino, Italy, Sep. 2010, Paper Tu.5.A.4.

[55] R. Nagarajan, M. Kato, J. Pleumeekers, P. Evans, D. Lambert, A. Chen, V. Dominic, A. Mathur, P. Chavarkar, M. Missey, A. Dentai, S. Hurtt, J. Bäck, R. Muthiah, S. Murthy, R. Salvatore, S. Grubb, C. Joyner, J. Rossi, R. Schneider, M. Ziari, F. Kish, and D. Welch, "Single-chip 40-channel InP transmitter photonic integrated circuit capable of aggregate data rate of 1.6 Tbit/s," *IEE Electron. Lett.*, vol. 42, no. 13, pp. 771–773, Jun. 2006.

[56] K. Prosyk, T. Brast, M. Gruner, M. Hamacher, D. Hoffmann, R. Millett, and K.-O. Velthaus, "Tunable InP-based optical IQ modulator for 160 Gb/s," presented at the European Conf. Optical Communication, Geneva, Switzerland, Sep. 2011, Paper Th.13.A.5.

[57] J. Telkkälä, J. Viheriälä, A. Aho, P. Melanen, J. Karinen, M. Dumitrescu, and M. Guina, "Narrow linewidth laterally-coupled 1.55 μm DFB lasers fabricated using nanoimprint lithography," *IEE Electron. Lett.*, vol. 47, no. 6, pp. 400–401, Mar. 2011.

[58] Y. Kang, H.-D. Liu, M. Morse, M. J. Paniccia, M. Zadka, S. Litski, G. Sarid, A. Pauchard, Y.-H. Kuo, H.-W. Chen, W. S. Zaoui, J. E. Bowers, A. Beling, D. C. McIntosh, X. Zheng, and J. C. Campbell, "Monolithic germanium/silicon avalanche photodiodes with 340 GHz gain-bandwidth product," *Nature Photon.*, vol. 3, no. 1, pp. 59–63, 2008.

[59] N. Keil, C. Zawadzki, Z. Zhang, J. Wang, N. Mettbach, N. Grote, and M. Schell, "Polymer PLC as an optical integration bench," presented at the Optical Fiber Communication Conf. Expo., Los Angeles, CA, Mar. 2011, Paper OWM1.

[60] D. van Thourhout, "Heterogeneous integration of III-V optoelectronic devices on silicon," in *Proc. 24th Int. Conf. Indium Phosphide Related Mater.*, Paris, France, May 2008, pp. 4703054-1–4703054-2.

[61] C. Kopp, S. Bernabe, B. B. Bakir, J.-M. Fedeli, R. Orobtchouk, F. Schrank, H. Porte, L. Zimmermann, and T. Tekin, "Silicon photonic circuits: On-CMOS integration, fiber optical coupling, and packaging," *IEEE J. Sel. Topics Quantum Electron.*, vol. 17, no. 3, pp. 498–509, May 2011.

[62] F. Smyth, C. Dorize, and W. van Heddeghem, "GreenTouch draft report on baseline power consumption," *GreenTouch Consortium*, Apr. 2011.

[63] R. S. Tucker, "Green optical communications—Part I: Energy limitations in transport," *IEEE J. Sel. Topics Quantum Electron.*, vol. 17, no. 2, pp. 261–274, Mar./Apr. 2011.

[64] InfiniBand Trade Association, Infiniband Architecture Specification, vol. 2, Physical Specification, Release 1.2.1, Oct. 2006.

[65] T. Tanimura, S. Oda, T. Tanaka, T. Hoshida, Z. Tao, and J. Rasmussen, "A simple digital skew compensator for coherent receiver," in *Proc. 35th Eur. Conf. Opt. Commun.*, Vienna, Austria, Sep. 2009, pp. 1–2.

[66] E. Frlan, F. Tremblay, and M. Li, "First demonstration of chip-to-module electrical channel interoperability over OIF CEI-28G-VSR compliant links," Gennum White paper 57278–0, Oct. 2011.

[67] V. Stojanović, "Channel-limited high-speed links: Modeling, analysis and design," Ph.D. dissertation, Stanford Univ., Stanford, CA, Sep. 2004.

Fotini Karinou was born in Arta, Greece, in 1983. She received the Diploma in electrical and computer engineering, with specialization in telecommunications and information theory, and the Ph.D. degree in optical communications from the University of Patras, Rio, Greece, in 2007 and 2012, respectively.

From October 2006 to May 2007, she was an Exchange Student at the Institute for Quantum Optics and Quantum Information at the Vienna University of Technology, participating in the initial attempts for the realization of a commercial prototype of a quantum key distribution system based on polarization entanglement. From June 2011 to December 2011, she was an Exchange Researcher at Denmark Technical University, the Photonics Department, where she worked toward optical interconnects and cognitive optical networks. Since February 2013 she has worked as an Optical Technology Researcher in the European Research Center, Huawei Technologies Duesseldorf GmbH, Munich, Germany. She has been involved in EU FP6 SECOQC, EU FP7 ICT-BONE, and EU FP7 CHRON projects.

Dr. Karinou has been a member of the Technical Chamber of Greece and a Student Member of the Optical Society of America since 2009.

Robert Borkowski was born in Lodz, Poland in 1987. He received the M.Sc. degree in telecommunications from the Technical University of Denmark, Kongens Lyngby, Denmark, in 2011 and the M.Sc. degree in electronics and telecommunications from the Technical University of Lodz, Lodz, in 2012. He is currently working toward the Ph.D. degree in the field of optical communications in the Metro-Access and Short Range Systems group at the DTU Fotonik, Department of Photonics Engineering, Technical University of Denmark.

He is involved in EU FP7 project Cognitive Heterogeneous Reconfigurable Optical Networks. His research interests include optical performance monitoring, coherent transmission systems, and digital signal processing for fiber-optic communications.

Darko Zibar was born in Belgrade, Serbia, on September 9, 1978. He received the M.Sc. degree in telecommunication and the Ph.D. degree in optical communications from the Technical University of Denmark, Kongens Lyngby, Denmark, in 2004 and 2007, respectively.

He was a Visiting Researcher with Optoelectronic Research Group, University of California, Santa Barbara, in January–August 2006, and also in January 2008 where he was involved in coherent receivers for phase-modulated analog optical links. From February–July 2009, he was a Visiting Researcher with Nokia-Siemens Networks where he worked on 112-Gb/s polarization multiplexed systems. He is currently an Associate Professor at the DTU Fotonik, Technical University of Denmark. His research interests include coherent optical communication, with the emphasis on digital demodulation and compensation techniques.

Dr. Zibar received the Best Student Paper Award at the IEEE Microwave Photonics Conference 2006, the Villum Kann Rasmussen Postdoctoral Research Grant in 2007, and Villum Foundation Young Investigator Program in 2011.

Ioannis Roudas (M'00) received the B.S. degree in physics and the M.S. degree in electronics and radio-engineering from the University of Athens, Athens, Greece, in 1988 and 1990, respectively, and the M.S. and Ph.D. degrees in coherent optical communication systems from the Ecole Nationale Supérieure des Télécommunications, Paris, France, in 1991 and 1995, respectively.

During 1995–1998, he was with the Optical Networking Research Department at Bell Communications Research (Bellcore), Red Bank, NJ. During 1999–2002, he was with the Photonic Modeling and Process Engineering Department at Corning, Inc., Somerset, NJ. Since 2003, he has been with the Department of Electrical and Computer Engineering at the University of Patras, Patras, Greece, as an Associate Professor of optical communications. He was an Adjunct Professor at Columbia University, the City University of New York, and the Hellenic Open University. He is the author or coauthor of more than 70 papers in scientific journals and international conferences and holds one patent. His current research interest includes spectrally efficient, multilevel modulation formats, adaptive electronic equalization, and optical interconnects.

Dr. Roudas serves as a Reviewer for the JOURNAL OF LIGHTWAVE TECHNOLOGY, IEEE PHOTONICS TECHNOLOGY LETTERS, IEEE JOURNAL OF QUANTUM ELECTRONICS, *Optics Express*, and *Optics Communications*. He is a member of the Optical Communications Subcommittee for the IEEE/LEOS Annual meetings in 2009–2012.

Kyriakos G. Vlachos received the Dipl.-Ing. and Ph.D. degrees from the National University of Athens (NTUA), Athens, Greece, in 1998 and 2001, respectively, both in electrical and computer engineering.

From 1997 to 2001, he was a Senior Research Associate in the Photonics Communications Research Laboratory (ICCS/NTUA). In 2001, he joined Bell Laboratories, Lucent Technologies, working in the Applied Photonics Group. In 2003, he was also a member of the Computer Engineering Laboratory of the Technical University of Delft, and since 2005 he has been a Faculty Member of the Computer Engineering and Informatics Department of the University of Patras, Patras, Greece. He is the (co)author of more than 120 journal and conference publications and also holds two international patents. His research interests include architectures and technologies for broadband, high-speed networks. He has participated in various research projects funded by the European Commission (IST-STOLAS, IST-PRO3, ESPRIT-DOALL, ephoton/ONe+, ICT-BONE, and ICT-DICONET).

Dr. Vlachos is a member of the Technical Chamber of Greece.

Idelfonso Tafur Monroy received the Graduate degree from the Bonch-Bruevitch Institute of Communications, St. Petersburg, Russia, in 1992, where he received the M.Sc. degree in multichannel telecommunications. He received the Technology Licenciate degree in telecommunications theory from the Royal Institute of Technology, Stockholm, Sweden, in 1996. He received the Ph.D. degree from the Department of Electrical Engineering, Eindhoven University of Technology, The Netherlands, in 1999.

He was an Assistant Professor at the Eindhoven University of Technology from 1999 to 2006. He is currently a Professor and the Head of the Metro-Access and Short Range Communications Group of the Department of Photonics Engineering, Technical University of Denmark, Kongens Lyngby, Denmark. He has participated in several European research framework projects in photonic technologies and their applications to communication systems and networks. He is currently involved in the ICT European projects GiGaWaM and EURO-FOS and is the Technical Coordinator of the ICT-CHRON project. His research interests include hybrid optical-wireless communication systems, high-capacity optical fiber communications, digital signal processing for optical transceivers for baseband and radio-over-fiber links, application of nanophotonic technologies in the metropolitan and access segments of optical networks as well as in short-range optical-wireless communication links.